Study of flow characteristics of a savonius turbine inside nozzle diffuser duct

DOI:10.36909/jer.15977

Shardul Vikram Singh, Pankaj Kumar*

Department of Mechanical engineering, SRM Institute of Science and Technology Kattankulathur, Chennai, TN, 603203, India

*Corresponding Author: pankajkr@srmist.edu.in

ABSTRACT

In the present study, flow characteristics of savonius hydrokinetic turbines are analysed numerically. CFD simulations are done for the savonius turbine with and without duct. A special design of nozzle-diffuser duct in the present simulation exhibits a higher performance of the turbine. The simulations are done at different TSR (Tip Speed Ratio) for which the torque coefficient (C_T) and Power coefficient (C_P) are compared for both the cases at constant Reynolds number (2.0×10^6). A significant increase of 64.65% in Power coefficient (C_P) is noticed for a ducted turbine when compared to a non-ducted turbine due to interesting vortices were formed in downstream of the duct.

Keywords: Savonius turbine; Nozzle; Diffuser; Power coefficient; Torque coefficient.

INTRODUCTION

In the present world, a lot of attention is given to reduce carbon emission and fossil fuels utilization. Since fossil fuels are not forever, huge importance is given to alternative sources of energy such as wind, hydrokinetic, solar, biomass, etc. Hydrokinetic is a ready source of energy available throughout the globe in abundance. Savonius turbines are used to produce power from the drag force of wind/water and are used widely due to many advantages over other turbines such as cost and reliability. Many research studies were done on savonius turbines in the past but

some important outcomes from the last decade is being discussed hereon. An unsteady flow analysis with CFD and PIV was done on savonius turbine by Dobrev and Massouh (2011). Measurement of instantaneous velocity at the centre was done using PIV and six different rotor positions were used to conduct the experiments. These experimental data were compared with the CFD simulations. Better results were observed in the case of 3D DES/K-ω model which represents the turbulent flow and thus, this approach can be used in the future. Patel et al. (2016) studied the role of Aspect Ratio (AR=Rotor height/Rotor diameter) and Overlap ratio (OR=Gap between two blades/Blade diameter) on a savonius water turbine and its performance. It was found that for smaller AR closed-ended vanes provided greater power coefficient compared to open-ended vanes. It was found that the maximum coefficient of power rises with an increase in overlap ratio by 66% for closed-ended vanes. Thus, a savonius hydrokinetic turbine with closed-ended vanes and 0.10 to 0.15 OR and AR greater than 1.8 could have the maximum power coefficient. Thakur et al. (2018) studied the effects of duct design with a jet on savonius water turbine's performance using Computational Fluid Dynamics. The simple turbine produced 17W whereas, the jet design produced 31W at the same current speed. The simple savonius turbine had a power coefficient of 0.35 at 0.64 TSR whereas the modified design had a power coefficient of 0.5 with a 0.61 TSR. The Experimental and CFD tests were carried out at low-velocity conditions and were compared with the Savonius turbine at the same speed by Sharma et al. (2014). It was learned that the torque and the power produced by the turbine increase exponentially as we increase the velocity of the flowing water, with the highest speed being 0.9 m/s. However, the increase in pressure will decrease the longevity of the turbine. The maximum C_P of 0.39 was at a TSR of 0.77 and this is much higher than the conventional savonius turbine. The hydrokinetic performance was greater by as much as 61.32% compared to the similar wind turbines at similar speeds. The suitable water velocity was calculated at 0.65 m/s to provide the perfect balance between the turbine's performance and longevity. The performance of a savonius

turbine with modified blades and deflectors was studied by Kailash et al. (2012). The savonius turbine has two deflector plates which aim to escalate the productivity of the turbine by making the drag coefficient larger and reducing the reverse force on the blade that is returning. The Savonius turbine blades were modified and kept straight in the end instead of the conventional curved design. For a single-stage modified turbine, the power coefficient without the deflector blades, at a TSR of 0.7 was found to be 0.14. By introducing the deflector plates, the C_P of the modified turbine increased to 0.21 at a TSR of 0.821. The appropriate position of the deflector plates was also determined by placing the plates at different positions and the maximum power coefficient improved to 0.35 at a TSR of 1.08. Similar things were reported by Singh et al. (2019) for variable speed in wind turbine.

A method to optimize the savonius turbine and reuse the wake energy was studied by Zhang et al. (2017). In the paper, the efficiency of a vertical axis savonius turbine is studied at optimal positions. To define the relationship between power coefficient and layout parameters the response surface model is established based on the Kriging method. The optimal position for advancing blade size was found to be x=5.23m and y=2.14m and ideal C_P (power coefficient) is 0.3044. There was an increase of 22.9% in the performance of the turbine in the most favourable position. Nag and Sarkar (2019) varied the duct angle and did an experimental and numerical study of its effects in the flow pattern and performance of a savonius turbine. For the study, three different types of turbines were used and compared with and without duct. The helical savonius hydrokinetic turbine generates the most power and torque, 1.58W and 0.26 Nm without duct. When a duct is added to the helical turbine then the power coefficient increases by 48.61% and coefficient of torque increased by 41.67%. The peak Power and Torque coefficients are 0.108 and 0.156 respectively at a TSR of 0.714. Different duct angles were also tested and it was found that with the increasing duct angle for 20, 23, 26, 29, and 32 degrees the power increases by 27.5%, 28%, 29%, 32%, and 34% respectively. Thus, with a higher duct angle the performance

of the turbine increases. Torres et al. (2011) did a 2D CFD analysis of a savonius turbine kept in an open field and also a closed test section and the results were compared. The CFD simulations were first carried out in an open field wind tunnel. It was discovered that the coefficient of torque of the turbine changed with respect to the tip speed ratio. When the TSR decreases, the torque coefficient also decreases. In a confined environment, it was found that the streamline interaction was much greater compared to the open field condition. Thus, in a confined condition, the performance of the VAWT turbine increased by 20% near the maximum power coefficient. The study on blockage effects on the performance of the turbine was done by Mauro et al. (2019). In the paper, influence of a duct on the turbine efficiency was studied by using 2D CFD model. The experimental and CFD investigation had similar results which are due to the satisfactory reliability and decent accuracy of the CFD model. It was noticed that the corrected C_P using pressure correction of the ducted turbine increased to 0.4 which is far greater than a conventional non-ducted savonius turbine without the duct. The study of ducted nozzle savonius water turbine and its comparison with conventional water turbine was done by Elbatran et al. (2017). In the study, a numerical investigation was performed for Reynold's Number equal to $1.32x10^5$. The proposed model was found to increase the flow of water to the advancing blade using ducted nozzle inlet turbine model. Compared to the basic modified savonius rotor the efficiency of the turbine increased by 78.0%

From the previous studies, we have noticed that the researchers have explored the different ways to improve the turbine efficiency. Some have modified the rotor shape and its dimensions whereas others used deflectors, put the turbine in a confined duct. Also, some research work on utilization of the wake, nozzle ducts to make savonius turbines more efficient. After careful examine all the studies conducted, there is a scope to increase the turbine output further by combining nozzle inlet with diffuser outlet. In the present study, a conventional savonius turbine inside a duct with a nozzle inlet and diffuser outlet is selected for the analysis. The CFD simulations are done for

different nozzle diffuser lengths and different area ratios. Based on the best torque output, the duct design is selected and used for further simulations at various Tip Speed Ratio (TSR). The vortex formation inside the duct is explained in detail with the velocity and pressure contours as well. Further, the Torque coefficient (C_T) and Power coefficient (C_P) are compared for ducted and non-ducted turbine models.

NUMERICAL METHODOLOGY

The conventional turbine structure is shown in Figure 1 which is used by Sun et al. (2012) in their two-dimensional simulation for the non-ducted turbine. Similar turbine is used here in the non-ducted and special design ducted case. The computational domain is kept 10 D upstream and 10 D downstream of turbine where D is Savonius rotor diameter. The convergent angle was kept 28 degrees for the flow uniformity at inlet. Three area ratios (A_1/A_2) were chosen as 2.26, 2.66 and 3.2. The non-dimensional length (L/D) was varying from3 to 5. The constant inlet velocity (v) of 2 m/s is applied at inlet-velocity and atmospheric pressure at the outlet. The rotating domain is allowed to rotate with different rotational speeds inside the stationary domain separated by interface with a rotor diameter of 1D similar to Sun et al. (2012). The different TSR (Tip Speed Ratios) were obtained depending upon the rotational velocity of the inner rotating domain. The Boundary conditions for ducted turbine and rotor structure are also kept same but the computational domain changes as shown in the Figure 2. A special Nozzle shaped inlet and Diffuser shaped outlet are made in a duct with the dimensions extending 10D upstream and downstream the turbine. Navier-Stokes equation is used for the unsteady simulation for the analysis. Unstructured mesh was used with fine mesh at the outer interface and inner rotating domain as shown in Figure 3. The face meshing is used to refine the mesh size in the inner rotating domain and edge sizing at the outer interface as the transition of mesh should be slow (1.1) for smoothness in adjacent elements. The inflation option of smooth transition with transition ratio 0.05 and growth rate 1.2 with 10 layers is provided. As the previous work of Sun et al. (2012), it

was found that the node number is 59008 is sufficient to capture the flow physics here so we have used medium sized mesh for the ducted turbine simulations. A grid independent study was conducted for TSR = 1 with different number of mesh elements for coarse (20000 elements), medium (35000 elements) and fine (60000 elements), shown in Figure 4. It was also extended for very high nodes (200,000) but the difference was not significant (Table 1). The K-ε RNG turbulence model with enhance wall treatment which is used in this study for all simulations as used by Sun et al. (2012) and average wall y+ near blade is found 32.

Number of cells	Torque coefficient	Fluid velocity (m/s) at point 1D from the turbine center towards nozzle.	% Change in Torque coefficient wrt reference	% Change in velocity wrt reference
20000 (coarse mesh)	3.36	4.73	18.30	9.23
35000 (medium mesh)	2.84 (reference)	4.33 (reference)	-	-
60000 (fine mesh)	2.81	4.51	1.05	4.15
200000 (veryfine mesh)	2.92	4.64	2.81	7.15

Table 1. Grid independent study for the ducted turbine

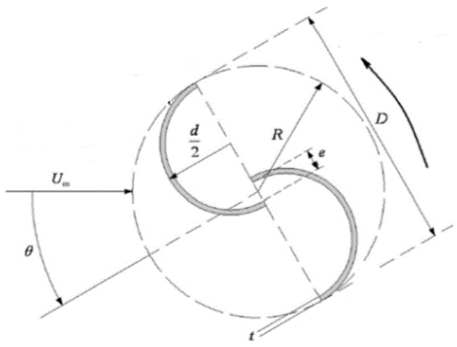

Figure 1. Design of a turbine rotor similar to Sun et al. (2012)

Continuity Equation:

$$\frac{\partial u_x}{\partial x} + \frac{\partial u_y}{\partial y} + \frac{\partial u_z}{\partial z} = 0 \qquad (1)$$

Navier-Stokes equation has the incompressibility assumption which reduces it to:

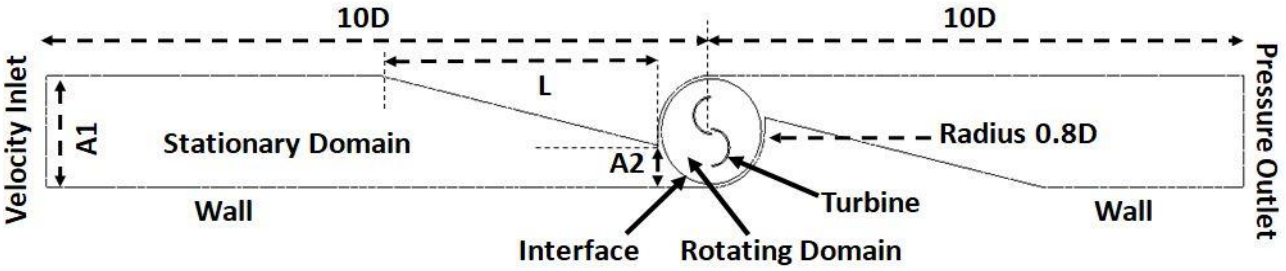

Figure 2. Computational domain of a ducted turbine

$$\frac{\partial(\rho u_x)}{\partial t} + u_x\frac{\partial(\rho u_x)}{\partial x} + u_y\frac{\partial(\rho u_x)}{\partial y} + u_z\frac{\partial(\rho u_x)}{\partial z} = -\frac{\partial \rho}{\partial x} + \mu\left(\frac{\partial^2 u_x}{\partial x^2} + \frac{\partial^2 u_x}{\partial y^2} + \frac{\partial^2 u_x}{\partial z^2}\right) \quad (2)$$

$$\frac{\partial(\rho u_y)}{\partial t} + u_x\frac{\partial(\rho u_y)}{\partial x} + u_y\frac{\partial(\rho u_y)}{\partial y} + u_z\frac{\partial(\rho u_y)}{\partial z} = -\frac{\partial \rho}{\partial y} + \mu\left(\frac{\partial^2 u_y}{\partial x^2} + \frac{\partial^2 u_y}{\partial y^2} + \frac{\partial^2 u_y}{\partial z^2}\right) \quad (3)$$

$$\frac{\partial(\rho u_z)}{\partial t} + u_x\frac{\partial(\rho u_z)}{\partial x} + u_y\frac{\partial(\rho u_z)}{\partial y} + u_z\frac{\partial(\rho u_z)}{\partial z} = -\frac{\partial \rho}{\partial y} + \mu\left(\frac{\partial^2 u_z}{\partial x^2} + \frac{\partial^2 u_z}{\partial y^2} + \frac{\partial^2 u_z}{\partial z^2}\right) \quad (4)$$

The formulas that are used for the calculation of:

Tip Speed Ratio,

$$TSR = \frac{\omega r}{v} \quad (5)$$

Power coefficient,

$$C_P = C_T\, x\, TSR \quad (6)$$

Where T is the rotor torque, ρ is the fluid density, ω is the angular velocity, v is the flow velocity and r is the rotor radius.

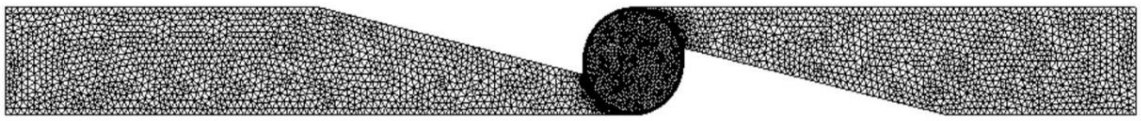

Figure 3. Unstructured mesh of the ducted turbine domain

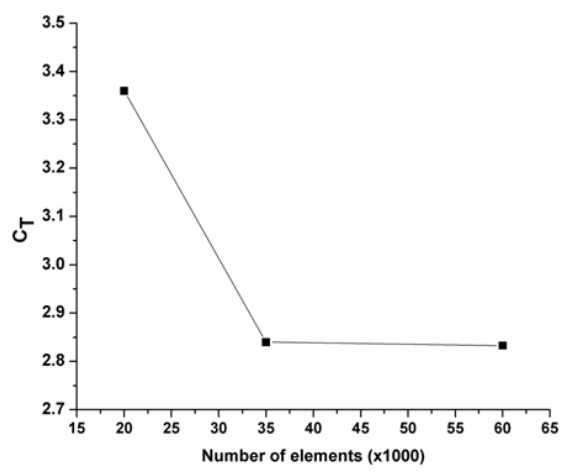

Figure 4. Grid Independent study for ducted turbine model

As the Torque coefficient does not vary much for medium and fine mesh as shown in Figure 4, The Non-ducted Savonious hydrokinetic turbine model was validated by CFD simulation using Ansys Fluent software. The similar rotor design and boundary conditions were used as in numerical study of Sun et al. (2012). The results for the present study for Torque coefficient (C_T) and Power coefficient (C_P) were compared with the results given by Sun et al. (2012),

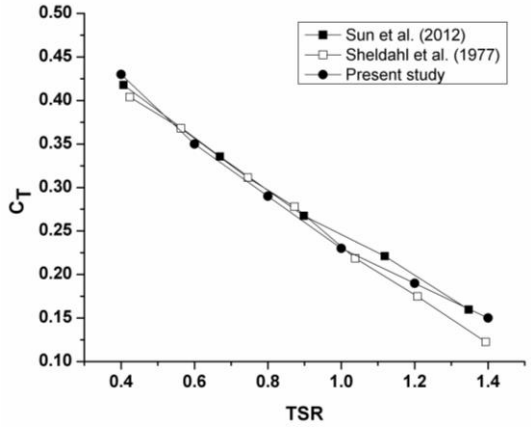

Figure 5. Comparison of the Torque coefficient (C_T) for non-ducted isolated turbine

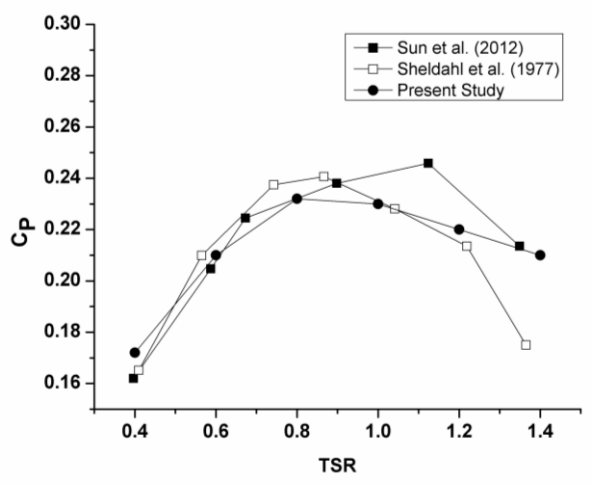

Figure 6. Comparison of the Power coefficient (C_P) for non-ducted isolated turbine

Sheldahl et al. (1977) at different TSR with proper validation as shown in Figure 5 and Figure 6. The SIMPLE algorithm is applied and equations are solved with second-order upwind scheme. The residuals were kept as 0.00001 for convergence of the equations.

RESULT AND DISCUSSIONS

ANALYSIS OF NON-DUCTED ABD DIFFERENT DUCTED TURBINE MODELS

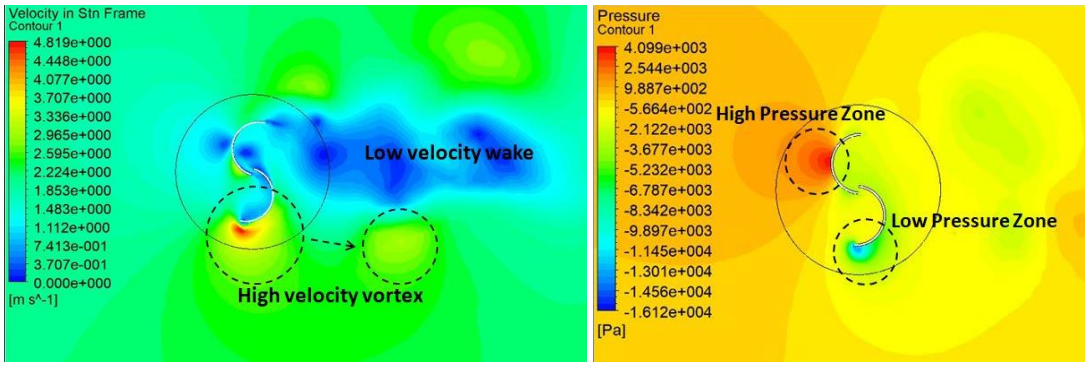

Figure 7. (a)Velocity and pressure distribution in a non-ducted turbine.

Figure 7 shows the velocity and pressure distribution for a non-ducted savonius turbine in which a low-velocity wake region is observed just downstream the turbine. Also, a high-velocity vortex is formed from the tip of the turbine which can be re-used to increase the performance of the

downstream turbines as a layout for multiple turbines as discussed by Zhang et al. (2017). It is observed that on the concave side of the advancing blade the high-pressure zone is formed whereas on the convex side of the advancing blade the low pressure zone is formed. And for the returning blade the high-pressure zone is formed on the convex side and low-pressure zone on the concave side. The pressure difference makes the turbine to rotate but also the higher pressure on the convex side of the returning blade creates negative torque.

ANALYSIS OF A NOZZLE-DIFFUSER DUCTED TURBINE

Different nozzle-diffuser duct designs were analysed by changing different design parameters of nozzle and diffuser. Nozzle-diffuser length (L) was changed for L = 3D, 4D, 5D and the ratio of inlet-outlet area for nozzle and diffuser for A1/A2 = 2.28D, 2.66D, 3.20D where A1 is kept constant and A2 is varied. For any particular case the dimensions of nozzle and diffuser are kept same for simulations. As shown in Figure 8 the C_T increases as the A1/A2 increases whereas C_T decreases with increase in length (L). So based on this analysis we used A1/A2 = 3.20 and L = 4D with nozzle-diffuser angle of 15.37˚ for the numerical simulations in this present study. The pressure distribution along the nozzle-diffuser ducted savonius turbine is shown in Figure 9(a) with a High-pressure region forming on the concave side of the advancing rotor blade as this part of the rotor is exposed to the high-speed fluid from the nozzle exit at 90˚ position where as this zone is pushed forward inside the diffuser as the rotor moves to the 180˚ position resulting in large low-pressure region with vortex formation inside the diffuser as also shown in Figure 9(b). The velocity vectors are shown for a ducted savonius turbine and the domain is divided into different zones with names A, B, C, D, E, F as shown in Figure 10(a). At 90˚ position, a vortex is formed in zone A, as a result of high-velocity inlet water moving from A to C through the convex side of the returning blade. Also, small vortices are observed at zone F. On further rotation of the turbine, the advancing blade pushes the water from zone D to the diffuser inlet and also

due to the blockage from the duct walls the pressure difference is created which accelerates the water inside the diffuser. The main reason for the formation of these re-circulating regions is that the high-speed fluid tries to move towards diffuser entrance around the rotating convex-concave shaped turbine due to the gap between the rotor and the circular outer duct domain and also due to the pressure differences due to turbine rotation. In Figure 10(c) the turbine moves to 180˚ forming a very high-speed rotating vortex inside the diffuser.

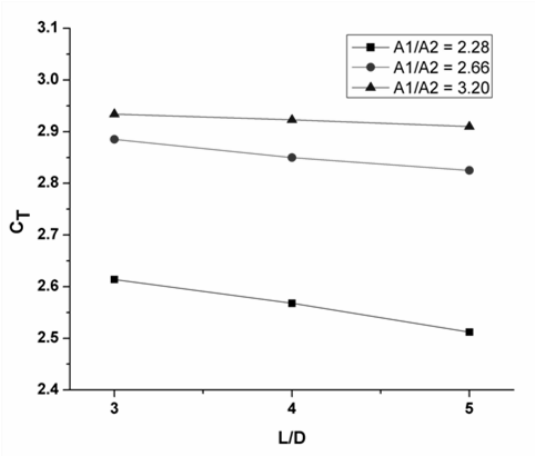

Figure 8. Comparison of the Torque coefficient (C_T) at TSR = 1 for ducted turbine with different design parameters

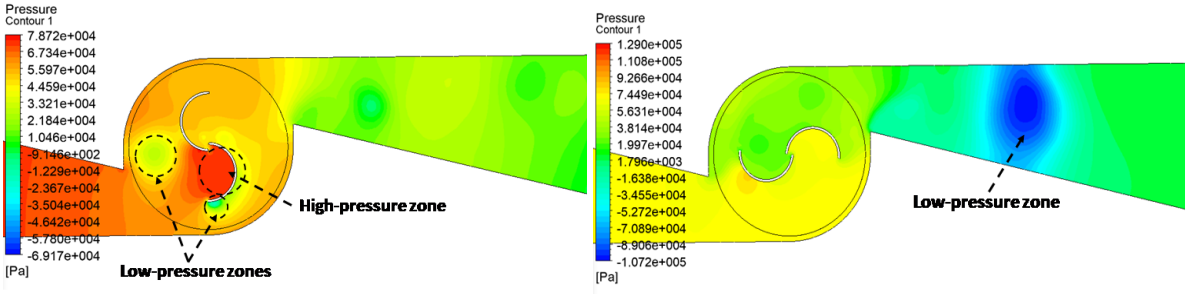

(a) 90˚ position (c) 180˚ position

Figure 9. Pressure contours at different positions during turbine rotation at rotor angle (a) 90˚ (b) 135˚ (c) 180˚

This is formed as the fluid velocity is very high in zone E relative to zone F and due to the shear force the fluid at zone F starts to flow in the backward direction forming a large high-speed vortex. Further turbine moving to 205˚ in Figure 10(d) the vortex in diffuser elongates and moves forward

creating a vortex street inside a diffuser. The periodic flow pattern is observed inside the duct for the consequent turbine revolutions.

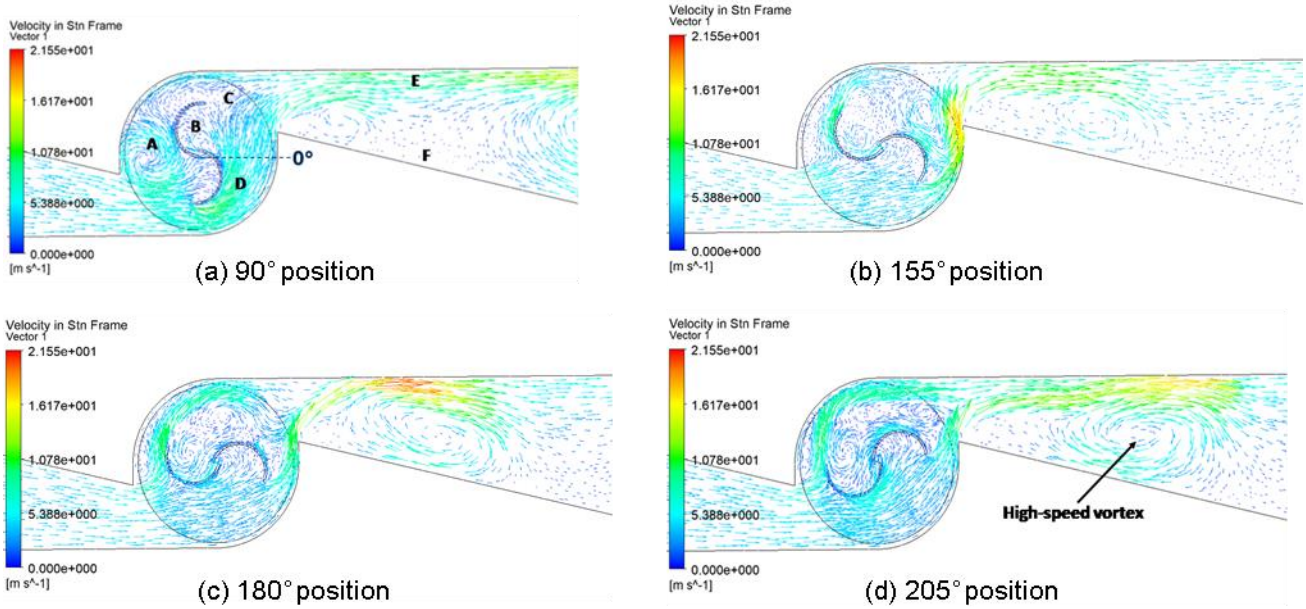

Figure 10. Velocity vectors at different positions during turbine rotation at rotor angle **(a)** 90˚ **(b)** 155˚ **(c)** 180˚ **(d)** 205˚ at TSR=1

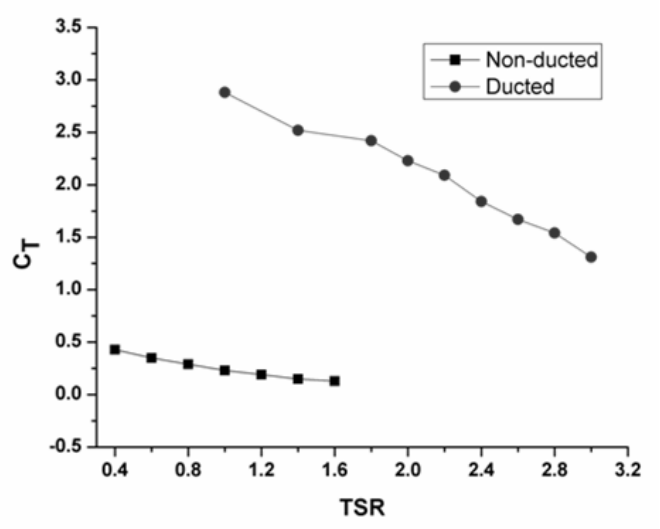

Figure 11. Torque Coefficient (C_T) for non-ducted and ducted turbines at different TSR

Figure 11 shows Torque coefficient (C_T) with significantly higher values for the ducted turbine in comparison to non-ducted turbine and Power coefficient (C_P) for ducted turbine is shown in Figure 12 and is calculated using formula (2) but this gives the misleading exceeded values of C_P as it must be below 1. This happens because Fluent calculates the C_P based only on Kinetic energy of fluid without considering the pressure effects due to blockage from the duct.

The Power coefficient (C_P) gives very high values for the ducted turbine which needs to be corrected using a formula as suggested by Mauro [14] given as:

$$\frac{P_e}{\frac{1}{2}\rho V^3 A + \dot{m}\frac{\Delta P}{\rho}} = C_P \qquad (7)$$

In the formula (7) P_e is the extracted power from the turbine, ρ is the fluid density, V represents the flow velocity, A= 1 m is the area of rotor section, mass flow rate is represented by $\dot{m} = \rho A V$ and ΔP is the pressure difference between upstream point and downstream point of the rotor. The fluid velocity at the upstream monitor point is around 4 m/s for all the cases which is used as flow velocity in formula (7).

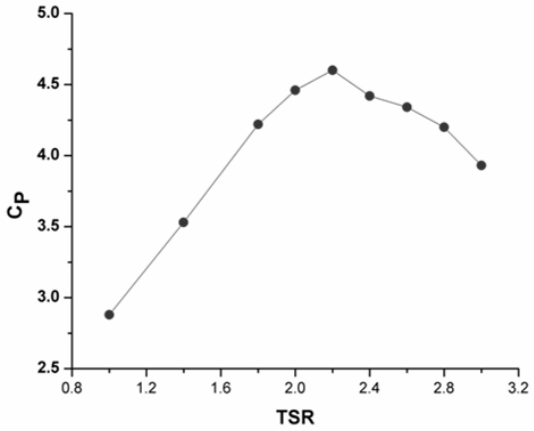

Figure 12. Power coefficient (C_P) [calculated] for ducted turbines at different TSR

The C_P plot for corrected values of ducted turbine using formula (3) is shown in Figure 13 compared with non-ducted case. The maximum value for non-ducted turbine is 0.232 at TSR=0.8 whereas for Ducted turbine it is 0.386 at TSR = 2.4. Therefore, the Nozzle-diffuser ducted turbine produced more power with increase of 64.65% in C_P.

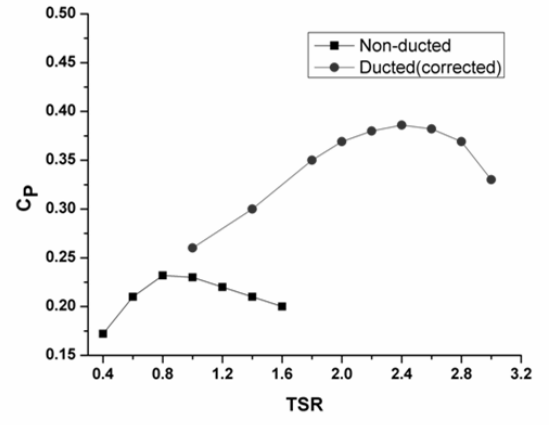

Figure 13. Power coefficient (C_P) for non-ducted and ducted [corrected] turbines at different TSR

CONCLUSION

The numerical investigation is done for non-ducted and nozzle-diffuser ducted turbine with same boundary conditions and some interesting results are observed. We found that there is large significance of inlet as well as outlet duct shape in the turbine output and flow structures. The highest C_T was observed for the nozzle-diffuser duct with L/D = 3 and A1/A2 = 3.20 but in the present study L/D = 4 is used as there is not much difference between them. The nozzle-diffuser ducted turbine resulted in 64.65% increase in power coefficient (C_P) in comparison to non-ducted turbine which is explained using pressure and velocity distribution inside a duct. Formation of high speed vortex is observed downstream the turbine inside the diffuser which can be used to increase the power output by placing another counter-rotating turbine placed after the diffuser exit section in further studies.

REFERENCES

Dobrev, I. & Massouh, F. (2011). CFD and PIV investigation of unsteady flow through Savonius wind turbine. Energy Procedia, **6**, 711-720.

Elbatran, A.H., Ahmed, Y.M. & Shehata, A.S. (2017). Performance study of ducted nozzle Savonius water turbine, comparison with conventional Savonius turbine. Energy, **134,** 566-584.

Kailash, G., Eldho, T. I. & Prabhu, S. V. (2012). Performance study of modified savonius water turbine with two deflector plates, International Journal of Rotating Machinery, **2012**, 1.

Mauro, S., Brusca, R., Lanzafame, R. & Messina, M. (2019). CFD modelling of a ducted savonius wind turbine for the evaluation of the blockage effects on rotor performance. Renewable Energy, **141**, 28-39.

Nag, A. K. & Sarkar, S. (2020). Experimental and numerical study on the performance and flow pattern of different Savonius hydrokinetic turbines with varying duct angles. Journal of Ocean Engineering and Marine Energy, **6**, 31-53.

Patel, V., Bhat, G., Eldho, T.I. & Prabhu, S.V. (2016). Influence of overlap ratio and aspect ratio on the performance of Savonius hydrokinetic turbine. International journal of energy research, **41**, 6.

Sarma, N.K., Biswas, A. & Misra, R. D. (2014). Experimental and computational evaluation of Savonius hydrokinetic turbine for low velocity condition with comparison to Savonius wind turbine at the same input power. Energy Conversion and Management, **83**, 88-98,

Sheldahl, R. E., Blackwell, B.F., & Feltz, L.V. (1977). Wind tunnel performance data for two- and three-bucket Savonius rotors. Sandia Report, SAND 76-0131.

Singh N., Bhanu P and Swarup A. (2019). Nonlinear robust observer based adaptive control design for variable speed wind turbine, Journal of Engineering Research, **7.** 258-284.

Sun, X., Luo, D., Huang, D., & Wu, G. (2012). Numerical study on coupling effects among multiple Savonius turbines. Journal of Renewable and Sustainable Energy, **4**. 053107.

Thakur, N., Biswas, A., Kumar, Y. & Basumatary, M. (2018). CFD analysis of performance improvement of the Savonius water turbine by using an impinging jet duct design. Chinese Journal of Chemical Engineering, **27 (4)**, 794-801

Torresi, M., Fortunato, B., Pascazio, G. & Camporeale, S.M. (2011). CFD analysis of a savonius rotor in a confined test section and in open field. Proceedings of ASME Turbo Expo. Power for Land, Sea and Air Conference, June 06-11, 2011, Vancouver, Canada.

Zhang, B., Song, B., Mao, Z. & Tian, W. (2017). A novel wake energy reuse method to optimize the layout for Savonius-type vertical axis wind turbine. Energy, **2**,121.